The Structure Sensitivity of Alkynol Hydrogenation on Shape- and Size-Controlled Pd Nanocrystals: Which Sites Are Most Active and Selective?

Micaela Crespo-Quesada,[†] Artur Yarulin,[†] Mingshang Jin,[‡]
Younan Xia[‡] and Lioubov Kiwi-Minsker[†,]*

[†]Group of Catalytic Reaction Engineering, Ecole Polytechnique Fédérale de Lausanne, 1015 Lausanne, Switzerland
[‡]Department of Biomedical Engineering, Washington University, Saint Louis, Missouri 63130, United States

Supporting Information

1. Atom type statistics for common fcc crystallite shapes

A non ideal model was chosen to estimate surface statistics of the nanoparticles used in this work. This model supposes the addition of an incomplete extra layer of atoms on the surface of the nanoparticle [1].

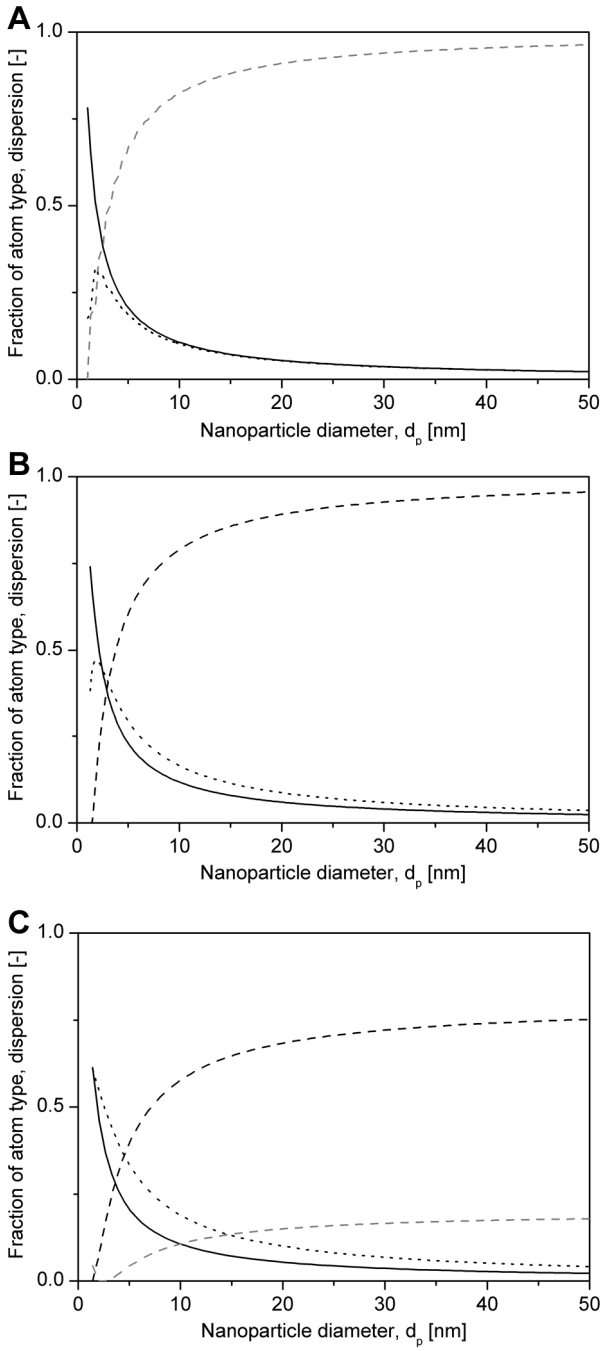

Figure S1. Dispersion (bold line), $Pd_{(111)}$ fraction (black dashed line), $Pd_{(100)}$ fraction (gray dashed line) and low-coordination (edge) atoms fraction (dotted line) as a function of the diameter for A) cubic, B) octahedral and C) cube-octahedral fcc nanoparticles.

2. HRTEM imaging and particle size distributions of the nanocrystals used in this work

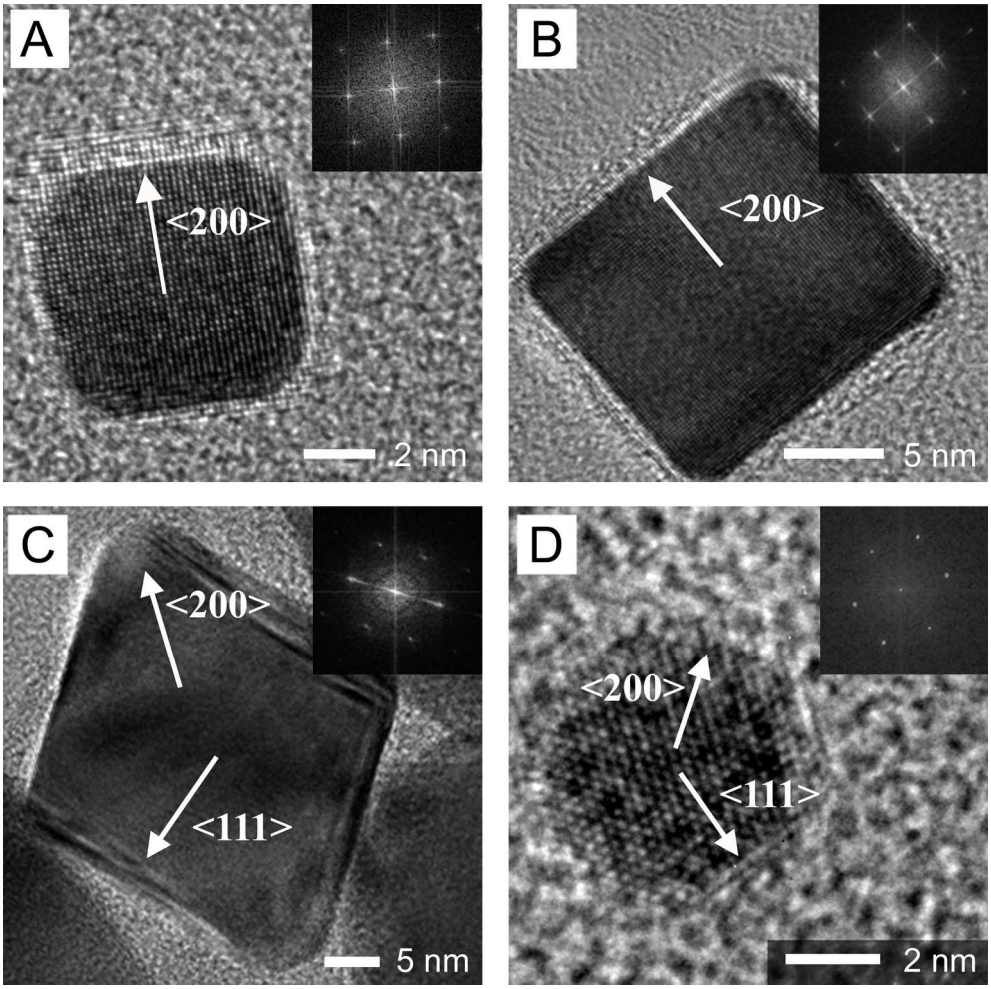

Figure S2. HRTEM images of the nanocrystals used during this study. A) CUB6, B) CUB18, C) OCT and D) COT. The inset in the figures show the FTT patterns of an individual nanoparticle where the lattice spacings can be indexed to reflections of face-centered cubic Pd as depicted in each panel.

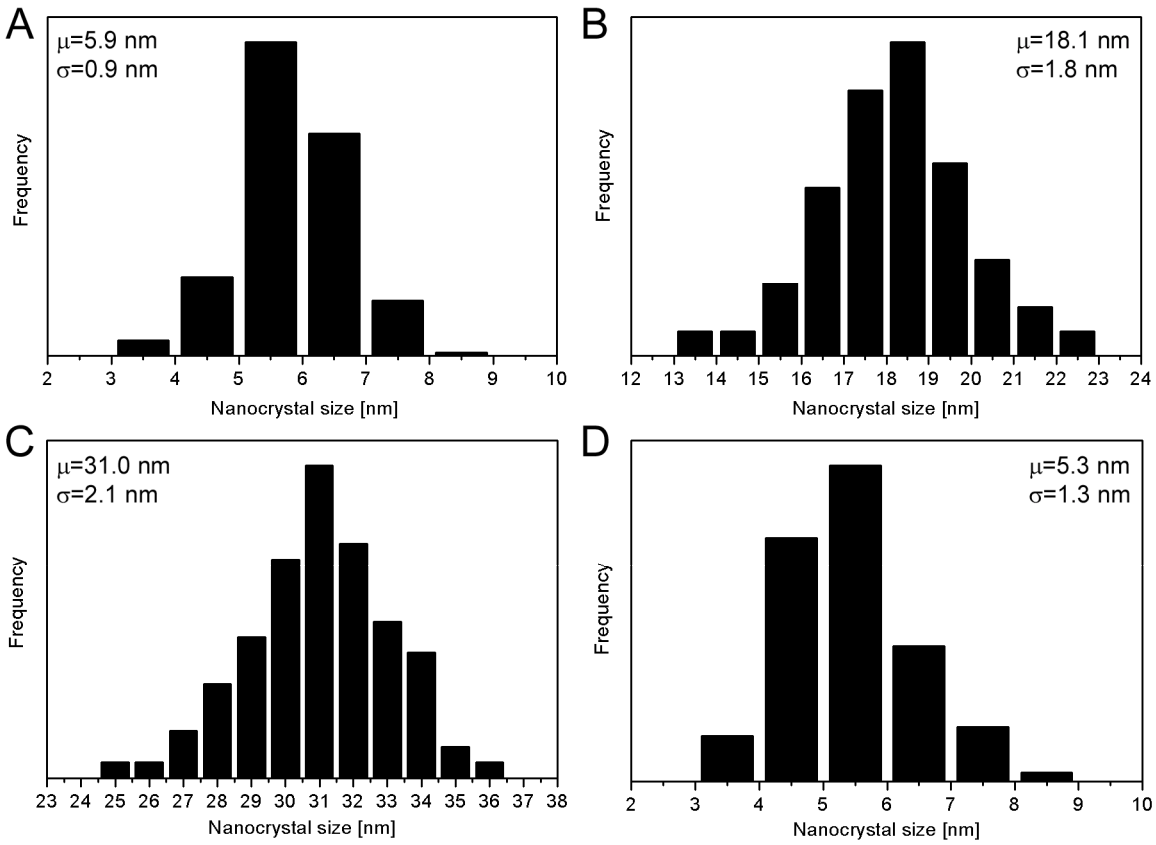

Figure S3. Particle size distributions of the nanocrystals used in this study. A) CUB6, B) CUB18, C) OCT and D) COT. In all samples, more than 95% of the nanocrystals presented the predominant shape.

3. XPS spectra of CUB6

In order to analyze the surface of the nanocrystals, they were first deposited on a carbon based support and they were subsequently analyzed as detailed in the experimental section of the manuscript. Figure S4 shows the XPS survey scan for CUB6 sample, where only C, O, Pd and N were detected. The spectra of the other samples were all analogous to that of CUB6.

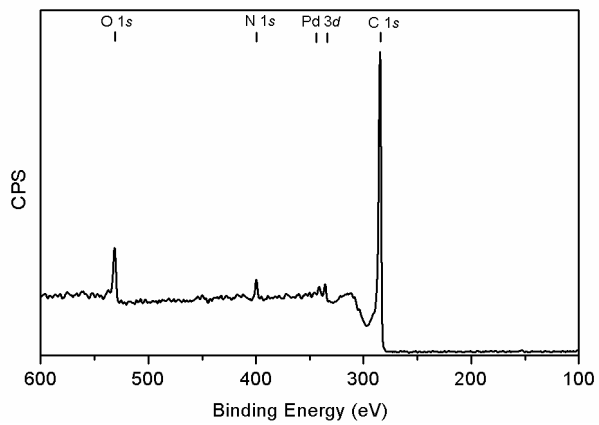

Figure S4. XPS survey spectrum for CUB6 sample, where only C, O, Pd and N were detected.

4. TEM image of cubic nanocrystals after a catalytic run

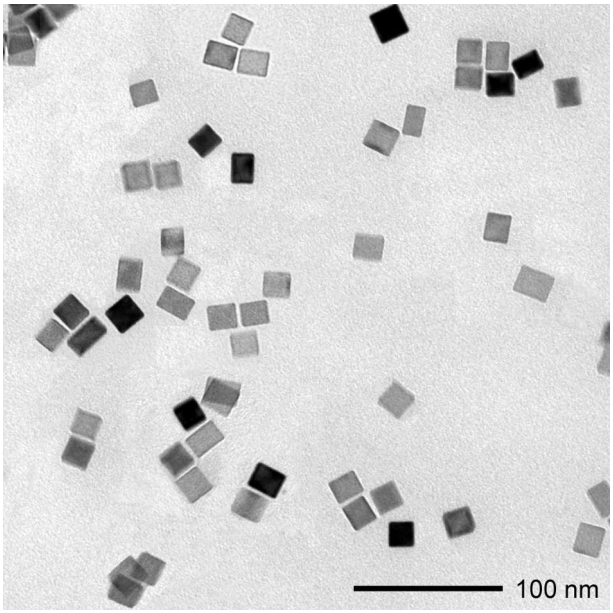

Figure S5. TEM image of cubic nanocrystals after a 2.5 h catalytic run, confirming that the morphology was well maintained.

5. Complete Langmuir-Hinshelwood mechanism for the hydrogenation of MBY

The series of elementary steps comprising the reaction network presented in Scheme 2 is listed in Table S1. The kinetic constant or reaction rate expression of each step is also included.

Table S1. Langmuir-Hinshelwood mechanism for the hydrogenation of MBY assuming two types of active sites.

Reaction	Site	Step		Kinetic expression
1 MBY→MBE (Y→E)	σ_1	1	$Y + \sigma_1 \xleftrightarrow{K_{Y,\sigma_1}} Y\sigma_1$	$K_{Y,\sigma_1} = \frac{\theta_{Y,\sigma_1}}{C_Y \cdot \theta_{\sigma_1}}$
		2	$H_2 + 2\sigma_1 \xleftrightarrow{K_{H_2,\sigma_1}} 2(H\sigma_1)$	$K_{H_2,\sigma_1} = \frac{\theta^2_{H,\sigma_1}}{C_{H_2} \cdot \theta^2_{\sigma_1}}$
		3	$Y\sigma_1 + H\sigma_1 \xleftrightarrow{K^*_{Y,\sigma_1}} Y^*\sigma_1 + \sigma_1$	$K^*_{Y,\sigma_1} = \frac{\theta_{Y^*,\sigma_1} \cdot \theta_{\sigma_1}}{\theta_{Y,\sigma_1} \cdot \theta_{H,\sigma_1}}$
		4*	$Y^*\sigma_1 + H\sigma_1 \xrightarrow{k_{1,\sigma_1}} E\sigma_1 + \sigma_1$	$r_1 = k_{1,\sigma_1} \cdot \theta_{Y^*,\sigma_1} \cdot \theta_{H,\sigma_1}$
		5	$E\sigma_1 \xleftrightarrow{K_{E,\sigma_1}} E + \sigma_1$	$K_{E,\sigma_1} = \frac{\theta_{E,\sigma_1}}{C_E \cdot \theta_{\sigma_1}}$
2 MBY→MBA (Y→A)	σ_1	1	$Y^*\sigma_1 + H\sigma_1 1 \xleftrightarrow{K^{**}_{Y,\sigma_1}} Y^{**}\sigma_1 + \sigma_1$	$K^{**}_{Y,\sigma_1} = \frac{\theta_{Y^{**},\sigma_1} \cdot \theta_{\sigma_1}}{\theta_{Y^*,\sigma_1} \cdot \theta_{H,\sigma_1}}$
		2	$Y^{**}\sigma_1 + H\sigma_1 \xleftrightarrow{K^{***}_{Y,\sigma_1}} Y^{***}\sigma_1 + \sigma_1$	$K^{***}_{Y,\sigma_1} = \frac{\theta_{Y^{***},\sigma_1} \cdot \theta_{\sigma_1}}{\theta_{Y^{**},\sigma_1} \cdot \theta_{H,\sigma_1}}$
		3*	$Y^{***}\sigma_1 + H\sigma_1 \xrightarrow{k_2,\sigma_1} A\sigma_1 + \sigma_1$	$r_2 = k_{2,\sigma_1} \cdot \theta_{Y^{***},\sigma_1} \cdot \theta_{H,\sigma_1}$
		4	$A\sigma_1 \xleftrightarrow{K_{A,\sigma_1}} A + \sigma_1$	$K_{A,\sigma_1} = \frac{\theta_{A,\sigma_1}}{C_A \cdot \theta_{\sigma_1}}$
3 MBY→MBE (Y→E)	σ_2	1	$Y + \sigma_2 \xleftrightarrow{K_{Y,\sigma_2}} Y\sigma_2$	$K_{Y,\sigma_2} = \frac{\theta_{Y,\sigma_2}}{C_Y \cdot \theta_{\sigma_2}}$
		2	$H_2 + 2\sigma_2 \xleftrightarrow{K_{H_2,\sigma_2}} 2(H\sigma_2)$	$K_{H_2,\sigma_2} = \frac{\theta^2_{H,\sigma_2}}{C_{H_2} \cdot \theta^2_{\sigma_2}}$
		3	$Y\sigma_2 + H\sigma_2 \xleftrightarrow{K^*_{Y,\sigma_2}} Y^*\sigma_2 + \sigma_2$	$K^*_{Y,\sigma_2} = \frac{\theta_{Y^*,\sigma_2} \cdot \theta_{\sigma_2}}{\theta_{Y,\sigma_2} \cdot \theta_{H,\sigma_2}}$
		4*	$Y^*\sigma_2 + H\sigma_2 \xrightarrow{k_{3,\sigma_2}} E\sigma_2 + \sigma_2$	$r_3 = k_{3,\sigma_2} \cdot \theta_{Y^*,\sigma_2} \cdot \theta_{H,\sigma_2}$
		5	$E\sigma_2 \xleftrightarrow{K_{E,\sigma_2}} E + \sigma_2$	$K_{E,\sigma_2} = \frac{\theta_{E,\sigma_2}}{C_E \cdot \theta_{\sigma_2}}$

4 MBE→MBA (E→A)	σ_2	1	$E\sigma_2 + H\sigma_2 \xleftrightarrow{K_{E^*,\sigma_2}} E^*\sigma_2 + \sigma_2$	$K^*_{E,\sigma_2} = \frac{\theta_{E^*,\sigma_2} \cdot \theta_{\sigma_2}}{\theta_{E,\sigma_2} \cdot \theta_{H,\sigma_2}}$
		2*	$E^*\sigma_2 + H\sigma_2 \xrightarrow{k_{4,\sigma_2}} A\sigma_2 + \sigma_2$	$r_4 = k_{4,\sigma_2} \cdot \theta_{E^*,\sigma_2} \cdot \theta_{H,\sigma_2}$
		3	$A\sigma_2 \xleftrightarrow{K_{A,\sigma_2}} A + \sigma_2$	$K_{A,\sigma_2} = \frac{\theta_{A,\sigma_2}}{C_A \cdot \theta_{\sigma_2}}$

* Rate Determining Step (RDS)

A surface balance of active sites must be performed in order to express site vacancies in terms of measurable parameters. The coverage of the intermediate species was neglected:

$$\theta_{\sigma_1} = \theta_{Y,\sigma_1} + \theta_{E,\sigma_1} + \theta_{A,\sigma_1} + \theta_{H_2,\sigma_1} \tag{S1}$$

$$\theta_{\sigma_2} = \theta_{Y,\sigma_2} + \theta_{E,\sigma_2} + \theta_{A,\sigma_2} + \theta_{H_2,\sigma_2} \tag{S2}$$

If coverages are expressed in terms of adsorption constants and bulk concentrations (obtained from Table S1):

$$\theta_{\sigma_1} = \frac{1}{1 + K_{Y,\sigma_1} C_Y + K_{E,\sigma_1} C_E + K_{A,\sigma_1} C_A + \sqrt{K_{H_2,\sigma_1} C_{H_2}}} \tag{S3}$$

$$\theta_{\sigma_2} = \frac{1}{1 + K_{Y,\sigma_2} C_Y + K_{E,\sigma_2} C_E + K_{A,\sigma_2} C_A + \sqrt{K_{H_2,\sigma_2} C_{H_2}}} \tag{S4}$$

Thus, the reaction rate expressions for all four paths of the mechanism can be developed and are presented in the manuscript as equations 4-7.

6. Kinetic modeling with one set of adsorption constants

Table S2. Adsorption and kinetic constants obtained during kinetic modelling of the studied samples.

Sample	Adsorption constants [L mol^{-1}]				Kinetic constants [mol mol^{-1}_{Pd} s^{-1}]			
	$K_{Y,\sigma1}$	$K_{Y,\sigma2}$	$K_{E,\sigma1}$	$K_{E,\sigma2}$	$k^*_{1,\sigma1}$	$k^*_{2,\sigma1}$	$k^*_{3,\sigma2}$	$k^*_{4,\sigma2}$
CUB6	20.5	56.5	0.2	2.7	10.0	0.3	0.6	12.8
CUB18					4.8	0.2	0.1	1.8
OCT					2.1	0.06	0.03	0.6
COT					9.3	0.2	1.7	19.3

It can be seen that the kinetic constant of the semi-hydrogenation of MBY to MBE on face sites is always higher than that of direct over-hydrogenation on face sites and of semi-hydrogenation on edge sites. However, the smallest samples, CUB6 and COT present a higher kinetic constant for the over-hydrogenation of MBE to MBA on edge sites. This can be seen in the experimental points (Figure S6), where over-hydrogenation takes place at relatively low conversion, when sites become available to MBE to undergo the over-hydrogenation. This is not observed on the largest samples, CUB18 and OCT, since despite that sites do still become available to MBE, it will adsorb mainly to face sites, where this reaction is not favored.

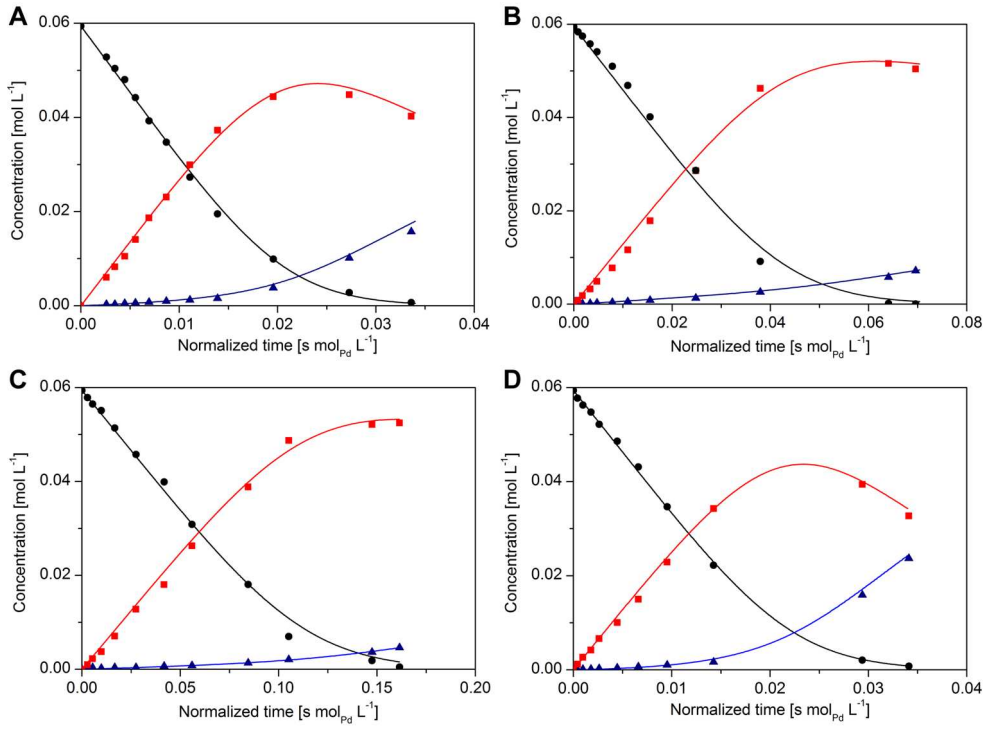

Figure S6. Experimental points for ● MBY, ■ MBE and ▲ MBA and prediction curves obtained by fixing the adsorption constants and varying the kinetic constants for each run for A) CUB6, B) CUB18, C) OCT and D) COT.

7. Kinetic simulations to estimate the productivity of MBE for different Pd nanocrystals

Figure S7 shows some of the simulation steps performed. In the case presented in Figure S7, the size of octahedral nanoparticles was varied between 3 nm and 50 nm. Over 200 simulations were run for this sample, but only 40 are shown in the figure for clarity reasons.

Figure S7A and S7B show the same variable, MBE concentration as a function of conversion and reaction time, respectively. They exemplify two possible ways of presenting the same information, only that Figure S7A is visually more straightforward with respect to maximum concentration of MBE. Figure S7C shows MBA concentration profile with respect to conversion, which is logically complementary to that of MBE. The combination of figures S7A and S7C derives in Figure S7D, which shows the selectivity of MBE expected for different sizes of octahedral nanoparticles, the lower curve corresponding to roughly 3 nm nanoparticles and the uppermost to 50 nm nanoparticles, respectively.

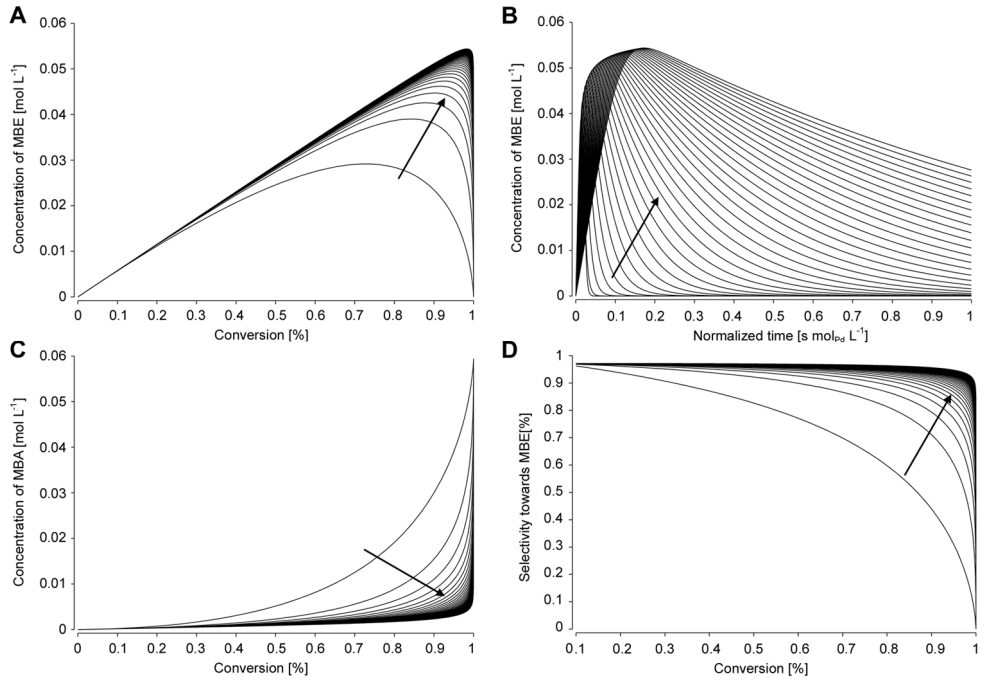

Figure S7. Some of the simulation steps performed for octahedral Pd nanoparticles. The arrows point towards increasing nanoparticle size. A) MBE concentration profiles as a function of conversion, B) MBE concentration profiles as a function of reaction time, C) MBA concentration profiles as a function of conversion and D) selectivity towards MBE as a function of conversion.

1. Van Hardeveld, R. and F. Hartog, *Statistics of Surface Atoms and Surface Sites on Metal Crystals.* Surface Science, 1969. **15**(2): p. 189-230.